The Effects of Particle Size on the Mechanisms of Atomization of Suspensions Using Hydraulic Spray Nozzles

F. O. Addo-Yobo
Research and Innovation Centre, Accra Polytechnic, P.O. Box GP 561, Barnes Rd, Accra, Ghana

M. J. Pitt
Dept. of Chemical and Biological Engineering, Sheffield University, Beech Hill Rd. Norton, Sheffield S10 2, U.K.

H. A. Obiri
The Institute of Industrial Research, CSIR, P.O. Box LG576, Legon, Accra, Ghana

DOI 10.1002/aic.12441
Published online November 8, 2010 in Wiley Online Library (wileyonlinelibrary.com).

A study of the effects of particles on the manner in which sheets of aqueous suspensions wetted particles disintegrate during atomization by hydraulic pressure nozzle showed that the sheet stability is reduced by particles in the region where the particle size is greater than the sheet thickness due to localized thinning of the sheet due to curvature variations caused by particles moving apart in this region. At high-volume fraction of solids, the sheets perforate. It is inferred from the mechanism that the critical volume fraction of solids at the onset of perforation decreases with decreasing particle size, decreasing density and surface tension, and increasing viscosity of the medium. A critical perforation number, A_c*, is inferred from the above mechanism. Waves are observed on the sheet at positions closer to the nozzle which would be absent on aqueous sheets similarly produced but free of particles.* © 2010 American Institute of Chemical Engineers *AIChE J,* 57: 2007–2024, 2011
Keywords: atomization, suspensions, liquid sheet disintegration, particles, critical perforation number

Introduction

To predict and control the important properties of sprays, e.g., drop-size distribution, produced by hydraulic pressure nozzles, it is necessary to understand the mechanisms by which the liquid sheets produced are atomized. In many instances, atomization is achieved by forming a thin freely moving sheet of liquid, using a nozzle, which subsequently breaks up to form droplets. When sheets are composed of single phase liquids, break-up occurs via action of aerodynamic waves. This mechanism is well understood, and there have been numerous reviews on it.[1] In contrast much less is known of the mechanism by which sheets composed of two phases break-up in spite of the obvious importance of such information for the spray drying industry where slurries and pastes are commonly sprayed to produce particles of desired physical properties. Chigier and Meyer[2] have pointed out that the break-up of sheets of slurries cannot be modeled on that of liquids free of particles. Dombrowski and Fraser[3] have reported that sheets of oil/water emulsions and also sheets of Fuller's Earth may spontaneously perforate before wave formation. Fraser et al.[4] have predicted the growth rate of perforations on sheets by equating the inertial and surface tension forces. These predictions have been confirmed in a series of papers by Spielbauer and Aidun[5] on the break-up of sheets of black liquor. The above workers[6] also provide

Correspondence concerning this article should be addressed to F. O. Addo-Yobo at waddoyob@hotmail.com.

an excellent account of the mechanisms of sheet disintegration. Mulhem and Schulte[7] have shown that particles play an important role in the disintegration of sheets of liquid suspensions.

As the presence of nonwetted entities (e.g., oil globules) can lead to sheet perforation, great care has to be taken to assure that all particles, used in this work are wetted during their residence in the sheet. To assure good wetting, the particles must be treated in such a way as to expose atoms which can undergo hydrogen bonding with water to the surface to reduce the contact angles below 90°.

In the 1980s, heuristic arguments were put forward attributing perforation to shear thinning behavior of the suspensions at the yield point. However, this seems unreasonable as the fluids undergo maximum shearing within the nozzle orifices and thereafter undergo elongational flow within the sheet at a strain rate, which reduces with distance from the nozzle. To buttress this point, we have made effort to ensure that suspensions with Newtonian and shear thinning rheologies are studied in the preliminary experiments.

Up to now, there remains a gap in the literature regarding the mechanism by which sheets perforate, which would enable quantitative verification. This article presents a mechanism by which relatively thick sheets can become destabilized due to curvature induced flow and investigates experimentally the influence of particle size and volume fraction of solids on the break-up of sheets of suspensions of wetted particles in liquids.

For experimental and theoretical reasons, the single orifice fan spray nozzle has been used to produce sheets. Liquid emerges from this nozzle in the form of thinning sheet, which subsequently breaks up into a spectrum of droplets.

Flow within the fan sheet is radial, and therefore, its thickness (H) reduces with increasing radial distance (R) from its apparent source behind the nozzle according to a hyperbolic law[8] shown in Eq. 1. K is the thinning parameter, which is a measure of how rapidly the sheet thins. K can be found empirically, as in this work, although it can be estimated from mass balance. It is determined mainly by nozzle geometry and only mildly depends on viscosity as the latter affects the distribution of flow within the nozzle orifice.

$$H = \frac{K}{R} \tag{1}$$

This system has features common to other types of atomizers such as the swirl spray and spinning atomizers.

A high-speed photographic technique has been used to record the effects of volume fraction of solids (phase ratio), on the disintegration of sheets of model slurries. A mechanism is proposed to account for the experimental observations.

The relevance of this work to the atomization literature lies in the identification of thinning mechanism induced by the presence of particles in the region where sheet thickness is less than that of the particles. A situation encountered in the combustion of solid fuel–liquid mixtures in many applications including rocketry. This work would enable a quantitative analysis of the influence of liquid properties on the perforation phenomena. Another important reason for reporting this work is that the break up of sheets containing suspended particles can be used to model the disintegration of sheets of shear thinning suspensions, which may be encountered in the food processing industry. The gel-like structure of such suspension can be expected to partially disintegrate into smaller domains or agglomerates on passage through the high-shear zones inside the nozzle orifice and therefore behave like discrete particles in a thin film.

Experimental

Choice of materials

The choice of materials used to form spray suspensions was informed by two considerations: discrete noninteracting particles offer a good way of uncovering the quantitative aspects of the mechanisms by which particles influence sheet disintegration. Suspensions formed from structure forming particles enable a demonstration of how widespread that underlying mechanism might be. Therefore, the screening experiments include both types of particles.

Interacting particles

Attapulgite. Particles of attapulgite clay comprise needle-like fibers of submicron diameter. These were suspended by introducing small quantities of it at a time into water with shearing action to form a thick suspension. Thereafter, the suspensions were stirred vigorously to enhance dispersion. The particles absorb several times their volume water on hydration and swell to form a smooth gel. The flow curve as determined by a Haake Rotovisco viscometer indicated that the gel (11% wt/wt) is shear thinning, with effective bulk viscosity reducing from about 6 cP, at low-strain rates, to about 1.5 cP in the higher strain rate regime. This response is indicative of the break down of the gel structure, formed on hydration, into smaller aggregates as the material is sheared.

Titanium Dioxide. Pigment-sized particles of titanium dioxide (TiO_2) were dispersed in water a little at time with shear action. The TiO_2 particles also absorbed large amounts of water on hydration to form a gel, which exhibited a typical shear thinning flow curve in the rheometer. This indicates that the gel structure breaks down on shearing into agglomerates (or gel-particles).

Noninteracting Particles. Three sets of glass particles of differing size distributions, shown in Figures 1A, B, and designated: coarse (Glass I), medium (Glass II), and fine (Glass III) of mean diameters 57 μm, 28 μm, and 5 μm, respectively, were used to prepare model suspensions of desired phase ratios. Clearly, these distributions are not monodisperse as would be required for the quantitative analysis particle size effects. Therefore, *Lycopodium* particles of near monodispersion (see Figure 1A), and average size 28 μm, are used to mimic the break up of sheets containing particles of Glass II for comparison. Glass and *Lycopodium* particles are noninteracting, and their suspensions exhibit Newtonian rheology.

The particles of glass were prewashed in chromic acid (to remove any oily substances and dirt) and rinsed in distilled water before being used to prepare the suspensions. The medium used was buffered water. Sprayed samples were collected and their weight fraction determined by drying thus ensuring that any errors due to deposition within the pipeline

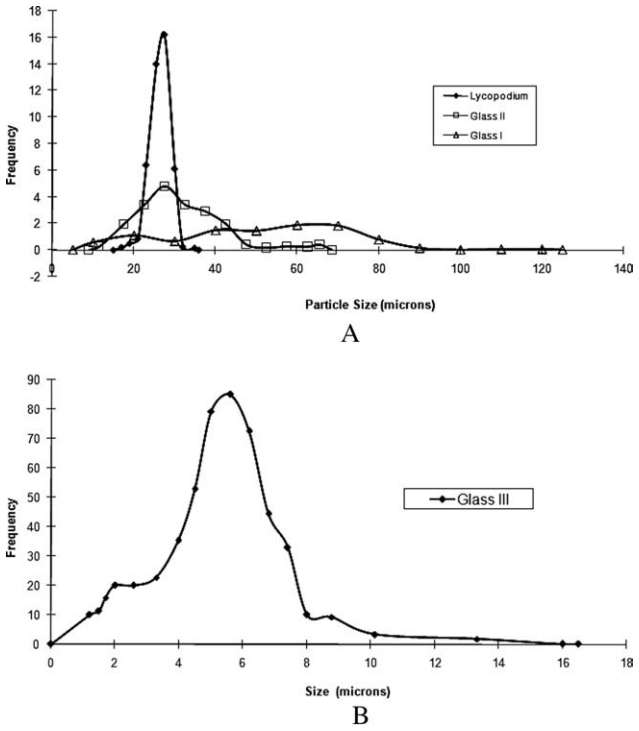

Figure 1. A: Size distribution of coarse particles; B: size distribution of fine particles of glass.

were avoided when interpreting the results. The volume fraction of solids (phase ratios) was deduced from the weight fraction and the known densities of suspension media and the particles. These results were corroborated by densitometer measurements.

Lycopodium particles as supplied were not wetted by water. To make them wet in water, the particles were heated (to temperatures from 70°C to boiling) to remove an oily substance from them into water, which could then be decanted. Such treatment exposes the surface cellulose of the seeds for bonding with water.

It is noted that it proved difficult increasing the phase ratios of coarse glass particles (especially particles of Glass I) much beyond 35% because the nozzle would block often leading to spitting. The main reason for this occurrence is the design of the chamber immediately above the orifice and the orifice geometry.

Sheets laden with discrete particles reported in this work are Newtonian, with effective viscosities less that 3 cP.

Spray System. The optical system incorporating the spray apparatus is sketched in Figure 2. The suspensions were stored in a pressure pot (upstream of the nozzle) and stirred agitated immediately before a run. Nitrogen at preselected pressures was used to force the suspensions through the nozzles. The sprayed slurry was collected in a tank and the particles recovered. The tank was extracted with a fan to maintain a gentle breeze of ambient air downward (in the direction of the spray) to prevent sprayed droplets from impinging on the sheets.

Technique and Atomizing Conditions. Atomizing pressures used ranged from 3 to 14 bars (see Table 1). The sheets were observed using a flash stroboscope and several photographs (at least five) were taken with a short duration (100 ns) light flash produced by an argon stabilized spark source, using focused rear illumination technique (Dombrowski and Fraser[3]).

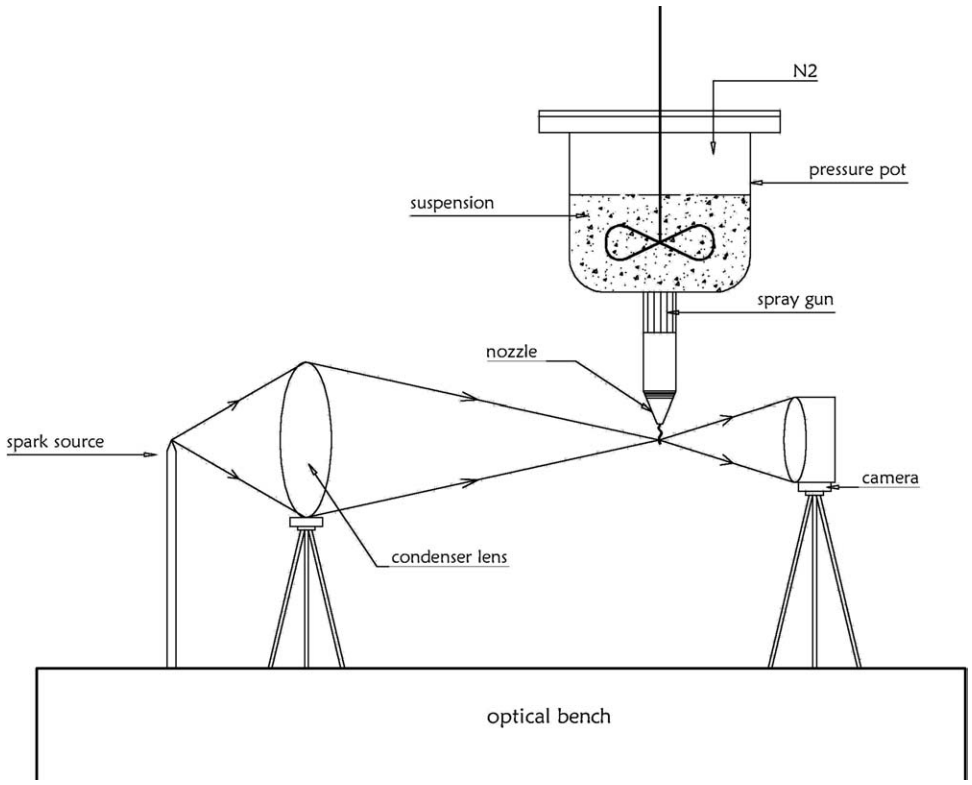

Figure 2. Optical system and spray unit.

Table 1. Nozzle Characteristics and Liquid Ejection Pressures Used in Experiments

Nozzle	Equivalent Spherical Diameter of Orifice (μm)	Spray Angle (°)	Ejection Pressure (bars)
Titan N519	480	50	3–14
Titan N521	533	50	3–14
Titan N943	1090	90	3–14
Titan N543	1090	50	3–10
Titan N243	1090	20	3–11

Dombrowski and Fraser[3] have reported that sheets containing nonwetted particles would perforate even at very low-volume fractions. Therefore, to confirm that particles were completely wetted during their residence in the sheet, photographs of sheets containing only a few particles of the solids were taken and inspected for perforations. Low-phase ratio sheets produced in this work did not perforate, confirming that the particles are indeed wetted.

The nozzles used in this work were selected carefully to ensure that undisturbed sheets could be produced over the range of operating conditions. Nozzles of equivalent orifice diameter 480–1090 μm and spray angle 20–90° (see Table 1) were used in forming sheets in the preliminary experiments. Once it was confirmed that the nozzles were not a direct cause of sheet perforation, nozzles designated N521 and N943 in Table 1, which had effective orifice diameters of 533 and 1092 μm, respectively, were selected for further work.

The thickness parameter of the sheets (K) produced were determined from their velocities and flow rate through a known width of sheet.[8] Nozzles N521 and N943 had effective thickness parameter of 17.2×10^{-8} m^2 and 27.4×10^{-8} m^2, respectively.

To determine the velocity of the sheet, double exposure photographs of the sheets were taken using the same film and the distance moved by the centre of features on the sheets in the known time interval between exposures recorded. The velocity of the sheet was calculated from the ratio of the distance moved to the time interval between exposures.

The amplitudes of the waves on the sheets were estimated from the shadow photographs of the side view of the sheets.

The radial lengths of the sheets at which perforation commenced were estimated by two complimentary techniques: from the growth rate of perforations and by extrapolating to the origin, the light streaks on the multiple exposure photographs caused by the axial movement of perforations.

Results

Wetting Properties of Particles. To demonstrate that all particles used in this work remained wetted throughout their residence period in the sheets (less than 3 ms), water containing very low concentrations of particles were used to form sheets, which were then observed. In all cases, the sheet lengths were not significantly changed and no perforations over the entire length of the sheet were observed. Figure 3A illustrates that the presence of a *Lycopodium* particles of size about 28 μm in a surrounding sheet of thickness 4.5 μm does not perforate it but instead the particle imposes curvature variations in its vicinity, which leads to high contrast over an area much larger than the cross section of the particles. The above result is entirely consistent with the earlier observation that once the oily component has been expelled from the *Lycopodium* seeds, they remain wetted by water molecules as strong hydrogen bonding would very easily form between the hydrogen and oxygen atoms in the cellulose in the surface of the seed particles and the hydrogen atoms in the free water molecules.

Figure 3B shows the presence of particles of size 56 μm (sampled from Glass I). These particles are wetted by the

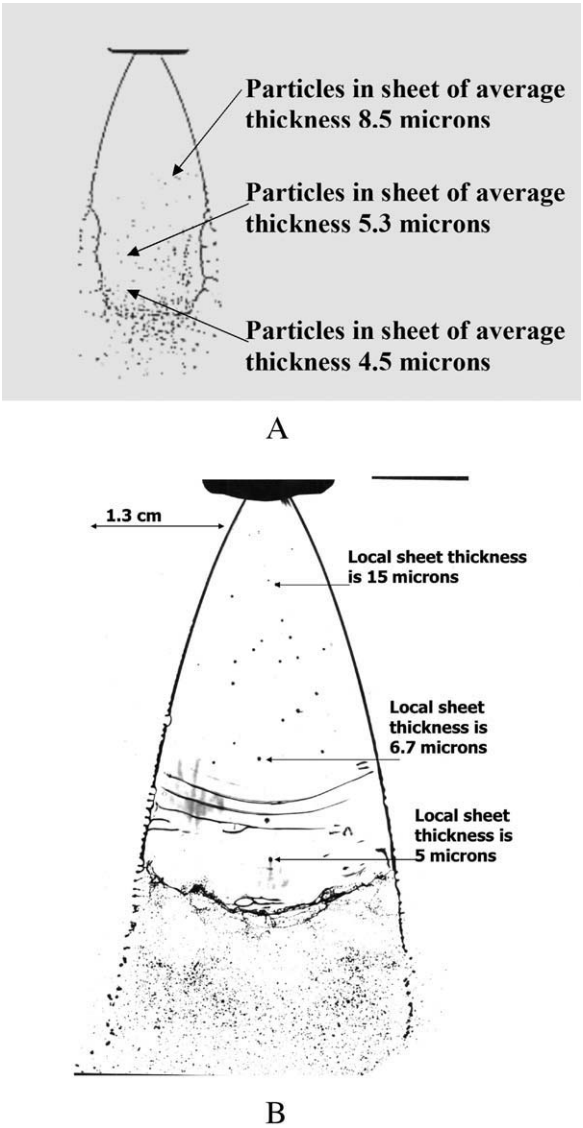

Figure 3. A: Particles of *Lycopodium* powder suspended in an expanding sheet of water; average local thicknesses of sheet are shown on the right-handed side (R.H.S.); B: particles sampled from Glass I suspended in an expanding sheet of water.

Average local thicknesses of sheet are shown on the R.H.S.

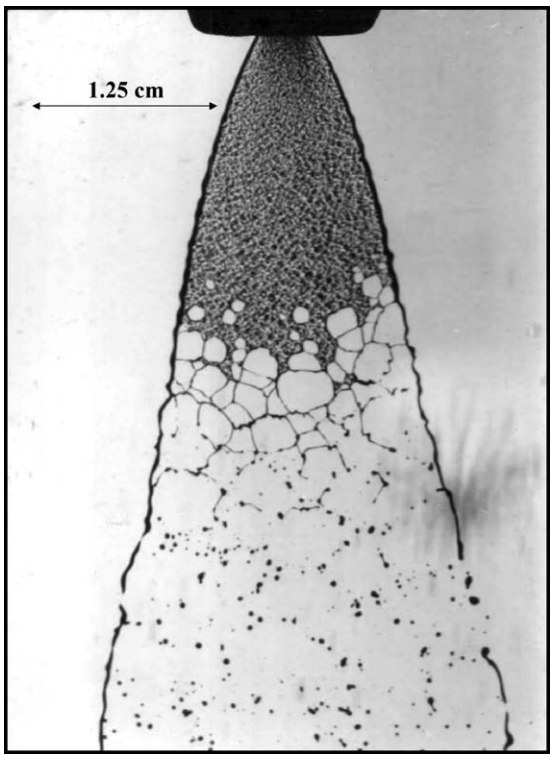

Figure 4. Perforated sheet of shear thinning suspension (11% attapulgite clay suspension in water).

sheet of water whose thickness reduces from 480 μm (close to the nozzle) to 3 μm (within the wave break-up zone). If particles did not remain wetted in the region where sheet thickness is less their size, then perforations would occur and grow, even at low-volume fraction of solid particles used here. In this case, also curvature variations imposed on the sheets have caused the particles to appear much larger in the sheets than they are.

Break-Up of Sheet Containing Structure Forming Particles. The breakup of sheets of attapulgite clay suspensions is superficially similar in some ways to the breakup of sheets containing discrete particles (e.g., *Lycopodium* and glass particles).

The sheets emerge from the nozzles and break-ups by perforating into a network of ligaments. The sheet thickness at the perforation distance is 12.5 μm, and the sheet thickness at the break-up distance is about 8.5 μm. Figure 4 illustrates this. The material in the sheet was sampled, as it emerged from the nozzle, into a dispersant solution to determine the agglomerate size using a traveling microscope. The sizes of the agglomerates observed were between 15 and 20 μm, which were dispersed in very fine suspensions. Thus, the sheet thickness at the perforation distance was less than the size of the largest agglomerates but thicker than the fines. The sheets are much shorter than the sheets of water produced by the same nozzle under similar atomizing conditions.

It was observed that the rims at the edges of the attapulgite sheets persist over a longer time—almost the entire length of the equivalent sheet free of particles—compared with the time in which the thinning sheets disintegrate. The networks of ligaments also persist for as long as 2 ms. This contrast with the break-up of the rim of sheets laden with discrete particles (cf. Figures 4 and 5C).

The break-up of sheets of titanium dioxides suspensions perforate in the region where the average sheet thickness is about 5.3 μm and where waves are present on the sheet. The perforations appear like tears and resemble the break-up of fine glass (Glass III) of size 5 μm. The sheet thickness at the break-up length is about 3 μm. The break-up characteristics

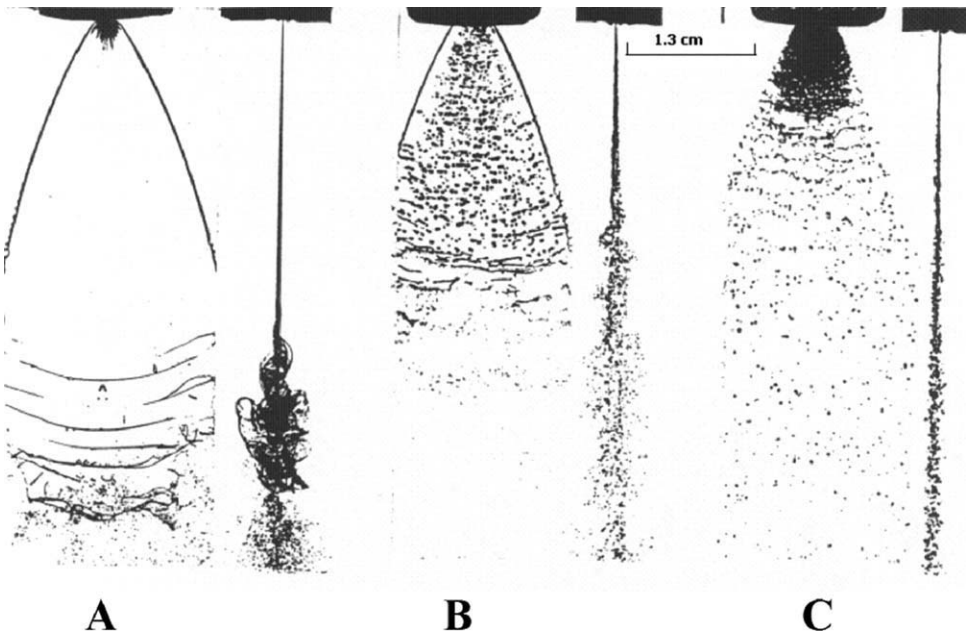

Figure 5. Front and side view of: (A) sheet of water free of particles breaking up due to the action of aerodynamic waves and aqueous sheet containing particles of Glass II (B) at low-phase ratio and (C) at high-phase ratio.

Table 2. Break-Up Characteristics of Sheets Containing Structure Forming Particles

Type of Particles	Nominal Size of Particles	Concentration of Particles (wt/wt %)	Sheet Thickness at Perforation Length (μm)	Sheet Thickness at Break-Up Point (μm)
Attapulgite	Submicron diameter	11%	12.5	8.5
Titanium	Pigment		5.3	3.5

Nozzle 521.

of attapulgite and titanium dioxide suspensions are summarized below in Table 2. Mass fractions have been used as a measure of the concentration of particles instead of the volume fraction, because it was not possible to determine the proportion of water that is chemically bonded to the solid matrices and that which is free.

The break-up of shear thinning (structure forming) suspensions would be interesting from the academic viewpoint and could also be used to mimic the sheet disintegration during the spray drying of starchy food. However, a lot more work would be required to characterize the break-up of the gels into agglomerates on passage through the high-shear zones in the nozzle orifice. Even after that is done, it would be a major problem to determine the proportion of water bonded within the gels and what percentage would be available within the inter-agglomerate space, which are important parameters in characterizing the state of the suspensions during their residence in the sheet . Therefore, greater effort is concentrated on sheets formed from suspensions of discrete non-interacting particles.

Disintegration of Sheets Containing Medium Sized Particles of Glass. To facilitate the presentation of the mechanistic aspects of this work, the break-up of a sheet of water is compared with the disintegration of sheets containing middle sized particles (Glass II) of average size 27 μm (see Figure 1A). Figure 5A shows a sheet of water containing no particles breaking up due to large amplitude aerodynamic waves as one would expect from conventional atomization theory as presented by Squire[9] and Hagerty and Shea.[10] In contrast, sheets containing particles of glass (II) of low-phase ratio break up via action of low-amplitude waves, which appear closer to the nozzle (illustrated in Figure 5B) compared with sheets of water free of particles. It is noted that the appearance of waves on sheets containing particles close to the nozzle, where they are not visible on sheets of water free of particles and produced under similar conditions, is unexpected and cannot be explained by conventional atomization theory.

Effect of Medium Sized Particles on the Structure of the Sheets. In the region of the sheets where the particle sizes exceed the local sheet thickness, as estimated by Eq. 1, the images of the glass particles in low-phase ratio sheets were much larger than expected and the particles of Glass II become visible on the photograph as black patches (see Figure 5B). Further down the sheet, image sizes (after correction for magnification) on the shadow photographs as large as 400 μm and above are observed, whereas in fact the largest size of particles sprayed was 65 μm (as measured by a particle size analyzer). This apparent magnification effect demonstrated more clearly on the photograph in Figure 3B, where the suspension is very dilute and the apparent diameter of the arrowed particle in the surrounding sheet of 5-μm thickness is about 450 μm. Therefore, its apparent magnification is eight-fold.

Stability Lengths of Sheets Containing Medium Sized Particles. At high-phase ratios (greater than a critical value defined later), the sheets perforate close to the nozzle beyond the region where the sheet thickness falls below the particle size (26 μm). A typical perforated sheet is shown in Figure 5C. The perforations grow as the rims thicken to form a network of ligaments, which subsequently disintegrate to into droplets. Striations can be observed on the sheets indicating the presence of low-amplitude waves. The side view of the sheets (see Figure 5C) showed the wave amplitudes in the perforated zones were so small that they are obscured by rims of the sheet.

Figures 5C and 6B show typical perforated sheets (of Glass II slurry) produced by two nozzles of different thinning parameter (K). Although perforation lengths differ, the sheet thickness at the onset of perforation (deduced from the Eq. 1) are equal within the experimental error of 10%.

The effect of the presence of particles in destabilizing sheets containing Glass II is summarized in Figures 7A, B which show the variation of both sheet break-up length and the perforation distance with phase ratio for two nozzles of orifice diameter 533 μm and 1090 μm, respectively. The break-up length is defined as the radial distance from apparent source of the sheet behind the orifice beyond which the sheet loses its connectivity. Curve C$'$ in Figure 7A shows that the break-up length of sheets containing Glass II falls steeply from 4.7 cm to 2.7 cm as phase ratio increases from 0–3.5% v/v. The reduction in sheet break-up length with increasing phase ratio is gentler at the higher values. The sheets perforate at high-phase ratios (beyond 17% v/v) and the perforation distance (curve D$'$ in Figure 7A) is relatively insensitive to phase ratio. The above results are confirmed by the break-up of sheets containing medium sized glass (II) particles, produced by a larger orifice nozzle (see Figure 7B), which produces sheets of larger thickness parameter—27.4 E -08 m^2. The sheet break-up length depicted in Figure 7B (curve A$'$) falls rapidly with increasing phase ratios (from 0 to ca. 15%) and then appears to level off at higher phase ratios. The perforation occurs at high-phase ratios (curve B) and the lengths are relatively insensitive to phase ratio at high values (dropping from 2.1 cm to 1.8 cm over an increase in phase ratio from about 20–27%).

Disintegration of Sheets Containing Lycopodium Particles. The above results indicate the importance of the size of particles relative to the local sheet thickness; therefore, *Lycopodium* particles of much narrower size distribution (see Figure 1) were used to mimic the impact of Glass II on sheet disintegration. Figures 8A–C illustrate the disintegration of

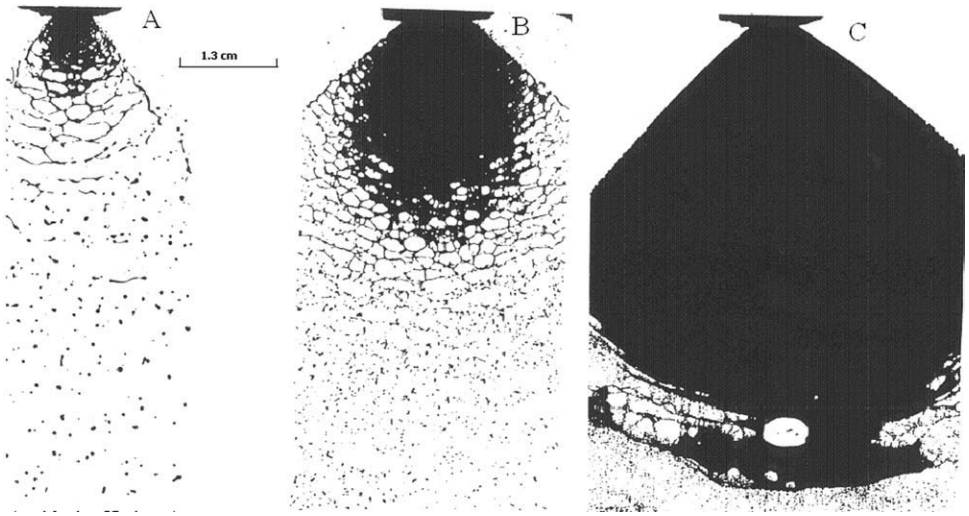

Figure 6. Perforated sheets of aqueous suspensions containing particles of different sizes (Sheet velocity 22 m/s, nozzle—N943).

sheets of water containing *Lycopodium* particles as a function of phase ratio. These sheets have been produced under conditions similar to experiments carried out on Glass II. It is noted in Figure 8B, that the *Lycopodium* particles appear much larger on the low-phase ratio sheets than their actual size (see arrowed features). This has been attributed to curvature variations caused by particles. The curvature effects begin at the radial distance where the sheet thickness is about 30 μm, which is close to the mean size of the particles. The apparent magnification of the particles within the sheet, inferred from the photographs, increased from 4 to 16 as the radial distance increases from 1 cm to 3.5 cm as shown in Figure 9 (curve A). Over those distances, the sheet thickness decreases from 18 μm to 5 μm as depicted in curve B in the same figure. This trend is brought about by presence of curvature variations in the area of the sheet surrounding the particles. These effects intensify as the sheets thin with distance from the nozzle because the curvature extends over a wider area as the sheet thickness reduces far below the size of the particles.

The perforations appeared on the *Lycopodium* sheets of high-phase ratio, at similar radial distance from the apparent source of the sheets as those containing particles of Glass II of high-phase ratio. The striations observed on the *Lycopodium* sheets are similar to those observed on the sheets containing Glass II.

In Table 3, the dependence of the perforation distances on the *Lycopodium* sheets on the ejection pressure are compared for different nozzles. It can be seen that four-fold variation in the ejection pressure (equivalent to doubling the sheet velocity) did not influence the perforation distance significantly. The same insensitivity was observed when nozzles of different thickness parameters were used. Thus, the speed of separation of particles (which is proportional to radial velocity) appears not to affect the kinetics of the perforation process greatly.

Curves E′ and F′ in Figure 7A show that the dependence on phase ratio of the break-up lengths and the perforation distance of sheets containing *Lycopodium*, follow a similar trend to that of sheets containing glass (II), but are not identical. At a given phase ratio, the break-up lengths of *Lycopodium* sheets are shorter than those of Glass II by about 0.25 cm. The curves depicting the variation of perforation lengths with phase ratio are almost coincident. Sheets of Glass II suspensions perforate at 17% phase ratio, whereas *Lycopodium* sheets perforate at 22% phase ratios. The differences may be attributed the presence of a significant proportion of glass particles of size greater than the mean in the distribution of the latter as shown in Figure 1.

In Figure 10, the maximum amplitude of waves in the break-up zone and the average thickness of the sheets at the break-up lengths are plotted against phase ratio (curves A and B). The amplitude of the waves in the break-up zone decreases from about 3 mm to 0.2 mm as phase ratio increases from 0% to 22%. Curve B shows the average thickness of the sheet in the break-up zone, calculated from the expansion flow, increases with increasing phase ratio from 3.7 μm (sheets free of particles) to 17.4 μm for sheets of phase ratio 22%. These results illustrate that the presence of particles in the region where sheet thickness is less than particle size, destabilize it to the extent that lower amplitude waves are able to break-up sheets of higher average thickness.

Disintegration of Sheets Containing Coarse Particles. The manner of disintegration of sheets containing glass of average size 57 μm (Glass I) is similar to the break up sheets containing Glass II as described above. The difference is that the perforation distance and the break-up lengths are closer to the nozzles, when the particles are larger. Comparison of photographs of sheets containing Glass I (A) and Glass II (B) in Figures 6A, B demonstrates these results effectively.

Curve C′ in Figure 7B shows the dependence of break-up lengths on phase ratio, of sheets containing Glass I produced by a nozzle of larger orifice diameter (N943). The break-up lengths fall with increasing phase ratio: steeply from 3.8 cm to 2 cm as phase ratio increases from 5% to 15% v/v. The break-up length then falls gently with phase ratios as the

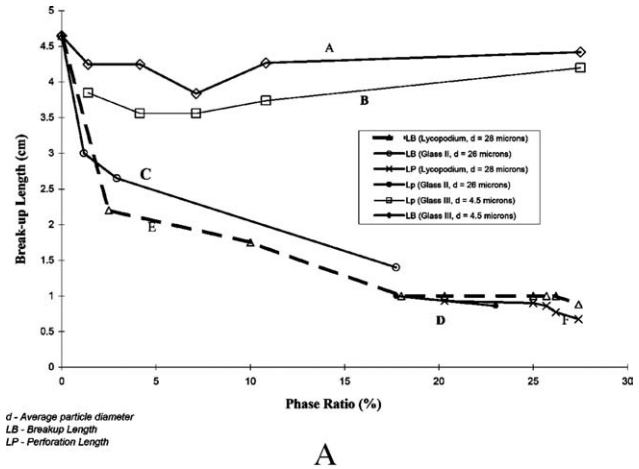

A

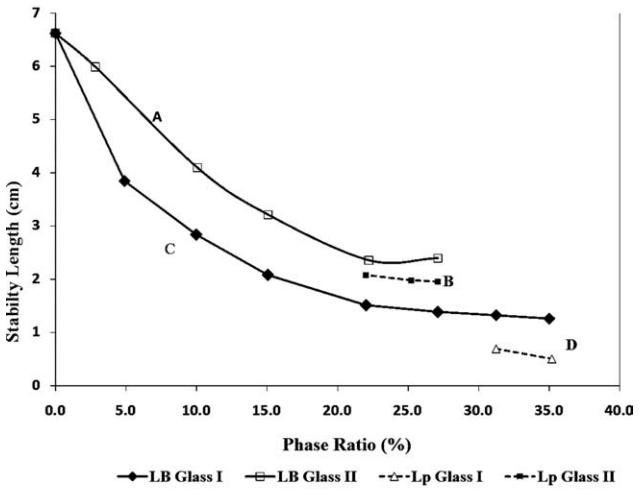

B

Figure 7. A: Stability length of sheets of suspensions of particles vs. phase ratio (v/v %) (Nozzle 521, sheet velocity 25 m/s); B: stability length of sheets of suspensions of particles vs. phase ratio (v/v %) (Nozzle 943, sheet velocity 25 m/s).

latter increases from 22% to 35%, for which the sheet length decreases from 1.4 cm to about 1 cm.

Perforation takes place at shorter radial distances from the source of sheet (e.g., see curve D′ in Figure 7B) and at higher phase ratios (in excess of 32% v/v) compared with sheets containing particles of Glass II (see curves A′ and B′ in Figure 7B).

Disintegration of Sheets Containing Fine Particles. Figures 6A–C show sheets containing coarse (Glass I), medium (Glass II), and fine (Glass III) particles, respectively. The sheets in the above photographs are of similar phase ratio and have been produced by the same nozzle. The perforation phenomena observed on the sheet containing fine particles is more intense and appears as tears (cf. Figures 6C with 6A and 6B). The break-up of sheets containing glass particles of average size 5 μm (Glass III) are also influenced by particles. At high-phase ratios, perforations occur on the sheets

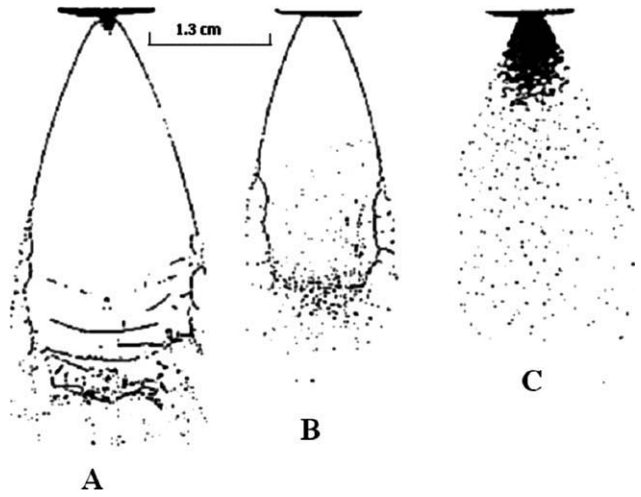

Figure 8. A: Sheet of water free of particles breaking up under the action of aerodynamic waves; B: sheet of water containing few particles of *Lycopodium* (0.11 v/v %) breaking up under the action of aerodynamic waves; C: sheet of *Lycopodium* suspension of high-phase ratio (25.0 v/v %) breaking up by perforation mechanism.

at radial distances from the nozzle where the sheet thickness is about 7 μm. Large amplitude aerodynamic waves are observed in same region. The perforation distance is subject to a degree of random fluctuations and the sheets are longer compared with sheets containing coarse particles (Glass I and Glass II).

The break-up lengths of sheets of Glass III decrease from 4.7 cm (no particles) to 3.7 cm (at 7% phase ratio) and increases gently with increasing phase ratio to 4.5 cm (at 27.5%) as shown by curves A′ in Figure 7A. The dependence of perforation distance on phase ratio follow a similar trend: it falls weakly with increasing phase ratio from 3.8 cm to 3.5 cm (at 7% v/v) then increases to 4.2 cm at 27.5% phase ratio. Over the range of phase ratios used, the maximum percent increase in sheet length was about 15%. This increase was accompanied by a reduction in the angle of emergence from the nozzle orifice at the higher values of the

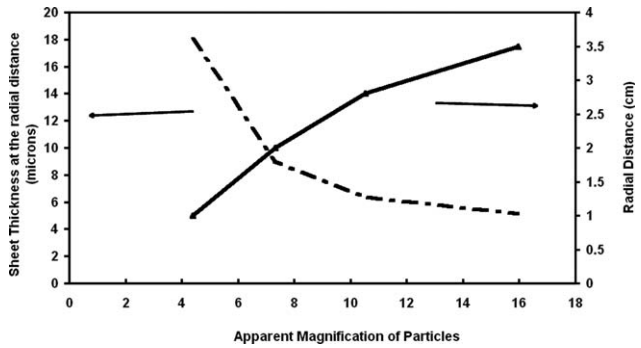

Figure 9. Apparent magnification of *Lycopodium* particles as function of sheet thickness and radial distance from the nozzle.

Table 3. Relative Insensitivity of Perforation Distance with Ejection Pressure

Thickness Parameter of Sheet (K)	Pressure (bar)	Perforation Distance (10^{-2} m)
17.2×10^{-8}	3.7	0.9
17.2×10^{-8}	4.1	0.86
17.2×10^{-8}	6.4	0.91
17.2×10^{-8}	13.6	0.98
27.4×10^{-8}	3.7	1.45
27.4×10^{-8}	7.1	1.55
27.4×10^{-8}	13.6	1.48
140×10^{-8}	4.1	7
140×10^{-8}	6.1	7
140×10^{-8}	11.2	7.3

phase ratio. Thus, there are changes in the sheet thickness parameter at the higher phase ratios and this relates to the flow field within the passages of the nozzle orifice. Because this work is not concerned with this issue, the measured radial distance, R_m, were corrected for any systematic changes in the measured thickness parameter (K_m) by equating sheet thicknesses to give:

$$R = R_m(K/K_m) \tag{2}$$

When these corrections are applied to the changes in perforation distance and break-up lengths, break-up lengths, and perforation distances were insensitive to phase ratio (beyond ca. 1.5% v/v) but subject to random fluctuations due to the presence of waves on the sheets.

Curve C in Figure 10 shows that the amplitude of aerodynamic waves in the break-up zone of sheets containing fine particles falls with increasing phase ratio, from about 3 mm (for sheets free of particles) and then levels off at about 1.3 mm, at phase ratios between 5% and 20%. The latter value is substantially larger than the amplitude of waves in the break-up zone of sheets containing coarse particles (cf. curve A in Figure 10), where wave amplitude in the break-up zone at 20% phase ratio is about 0.5 mm). The corresponding

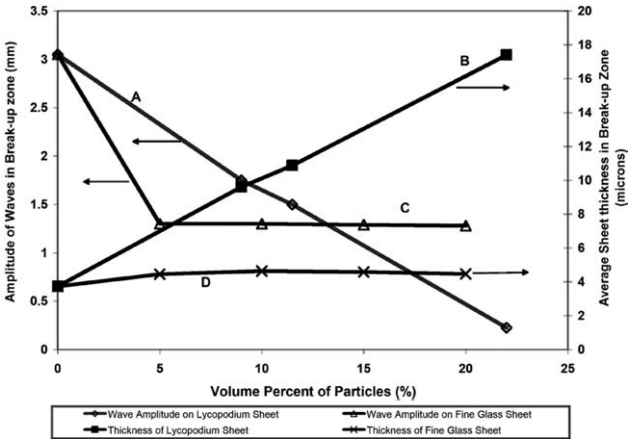

Figure 10. Amplitude of waves in break-up zone and the average thickness of sheets of suspensions at the break-up distance vs volume fraction (phase ratio) (Nozzle 521, velocity ca. 25 m/s).

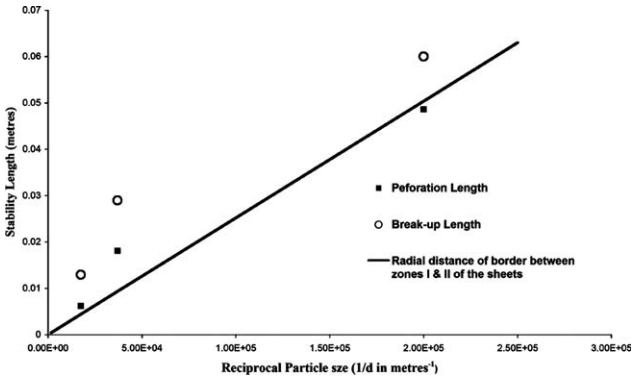

Figure 11. Summary of the dependence of stability length on particle size.

sheet thickness in the break-up zone increases from about 3.7 μm to about 4.5 μm as phase ratio increases from 0 to 20% (see curve B in Figure 11). Thus, the presence of fine particles do reduce the stability of the sheets, but to a lesser extent that the reduction in stability due to coarse particles.

Table 4 summarizes the effects of particles size on the appearance of waves of significant amplitudes, on sheets of suspensions of glass of three particles sizes. The minimum radial distance, from the source of the sheet, beyond which waves can be seen on the sheets produced by two nozzles, of different thickness parameter (i.e., different orifice size and spray angle), are compared with the radial distance at which the sheet thickness falls below the particle size in Table 4. For the entire range of particles sizes, wave action can be seen on the sheets at shorter distances from the nozzle orifice when particles are present compared with the case when the sheets are free of particles. Examination of columns three and four of the above table shows that large amplitude waves could be seen at radial distances where sheet thicknesses are greater than particle size when the sheets contain fine particles (Glass III). The opposite is the case, when sheets contain large particles (Glass I and Glass II).

Summary of particle size effects on the stability lengths

In Figure 11, the perforation lengths of the sheets produced by a typical nozzle (N943) under standard conditions are plotted against the reciprocal of the particle diameter. The radial distance from the nozzle at which the sheet

Table 4. Comparison of Minimum distance from Nozzle at Which Waves are Visible with the Distance at Which Sheet Thickness Falls Below Particles Size

Titan Nozzle Type	Particle Size (μm)	Distance from Nozzle at Which Sheet Thickness Equals Particle Size (cm), K/dp	Distance from Nozzle at Which Waves are Visible (10^{-2} m)
N521	No particles	Not applicable	3.3
N521	4.5	3.9	2.3
N521	27	0.64	1.1
N943	No particles	Not applicable	3.5
N943	4.5	6.0	3.2
N943	27	1.0	2.1
N943	55	0.49	0.62

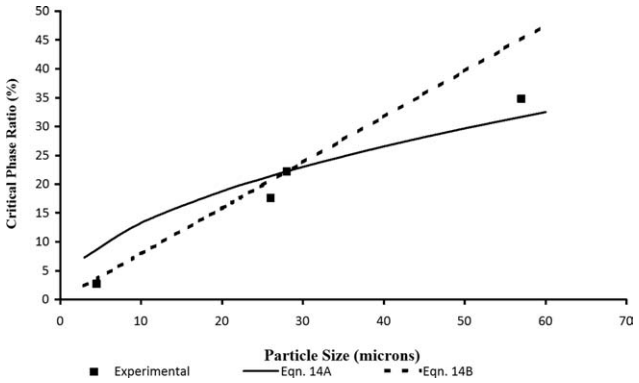

Figure 12. Critical phase volume fraction of solids (phase ratio) at the onset of sheet perforation vs Size of suspended particles.

thickness falls below the particle size (as predicted by Eq. 3) is shown on the same graph. It is apparent from the above that perforations occur closer to the nozzles as the size of particles increase. The experimental points lie close to the theoretical line. Even though these glass particles are not monodisperse, they are nonetheless unimodal in their distribution and also rounded in shape; therefore, the average particle diameter has been used to represent particle size.

It is apparent from the above figure that the sheet break-up length (L_B) decreases with increasing particles size; however, the relationship is nonlinear.

Dependence of critical phase ratio on particle size

It is noted that for each of the three particle sizes used, there exist a threshold phase ratio—critical phase ratio above which perforations could be seen on sheets. This critical phase ratio is insensitive to the range of atomizing velocities used and the nozzle used. Dombrowski and Fraser[3] also report that the perforation of sheets of Fuller's earth is not affected by the nozzle or atomizing pressure used. Figure 12 shows the variation of this critical phase ratio with particles size. The critical phase ratio increases from about 2% v/v for particle size of 5 μm to about 35% for particles of size 55 μm. These results were neither affected by the nozzle used nor the atomizing pressure as the latter was varied from 3 bar to 14 bar.

Finally, we note that although this article does not seek to account for droplet sizes resulting from the sprays, comparisons of photographs of sprays formed from sheets containing coarse and fine particles showed qualitatively that the former produced larger particles compared with the latter (cf. Figures 6A–C).

Effect of mixed particle sizes

As stated earlier, the presence of larger diameter particles introduce curvature variation effects on the sheet closer to the nozzle where the sheet is thicker compared with the case where only smaller sized particles are present. Therefore, it can be expected that a small number of relatively large particles can be introduced into a distribution of predominantly smaller particles to change the character of the sheet disintegration. In a demonstrative experiment, a suspension of a mix comprising 7.3 v/v % fine glass (Glass III) and 1.7 v/v % coarse glass (Glass I) used to form a sheet its disintegration observed. As recorded in Table 5, sheets containing 1.7% coarse glass do not perforate but have a long break-up length (ca. 6.5×10^{-2} m); sheets laden with fine glass (III) of strength 7.3 v/v % (which is greater than the critical value), perforate at a large distance from the nozzle (ca. 5×10^{-2} m) and the break-up length is about 1 cm longer. In sharp contrast, sheet comprising the majority fine glass particle dosed with 1.7 v/v % coarse glass perforated close to the nozzle (at radial distance of 1.25×10^{-2} m where the sheet thickness is 22 μm. Likewise the break-up length, the same sheet is short (about 1.5 cm).

Such apparently unusual results cannot be explained by any unusual rheological effects because the volume fraction of solids is small—and, therefore, the fluid rheology is Newtonian and close that of water. Particle dewetting is also not an issue. Rather, they can be inferred from the mechanism of curvature driven thinning of the sheet as outlined above. The large particles thin the sheet in the interparticle space to the size of the smaller particles (5 μm). Because these smaller particles are present in volume fractions which exceed the critical value, the sheets perforate and break-up closer to the nozzle than expected.

Discussion

The experimental results show that particles reduce the stability of freely moving sheets of suspensions. The reduction in stability takes the form of perforations, which appear on the sheets and grow, and the accelerated growth of waves in the region where conventional atomization theory would lead one to expect otherwise. As there is no accepted rational theory which would explain many of these seemingly paradoxical results, this section is prefaced by a discussion of hypotheses, which could be advanced to explain the above observations, followed by their elimination and further discrimination.

Particle dewetting hypothesis

As stated earlier, when nonwetted particles or liquids are suspended in thinning freely moving sheets of water, spontaneous perforations can take place, even at low-phase ratios

Table 5. Impact of Large Particles on the Break-Up of a Sheet of Suspension of Fine Particles

Description	Size Range (μm)	Critical Value of Volume Fraction	Actual Volume Fraction	Perforation Length (10^{-2} m)	Break-Up Length (10^{-2} m)
Coarse glass	10–90	35%	1.7%	Not applicable	6.5
Fine glass	1.3–13	3.5%	7.3%	4.9	6.0–6.35
Mixture:	1.3–13 and 10–90		Coarse glass: 1.7% Fine glass: 7.3%	1.25	1.50

Nozzle characteristics: code N943, diameter 1090 μm, $K = 27.4 \times 10^{-8}$ m^2.

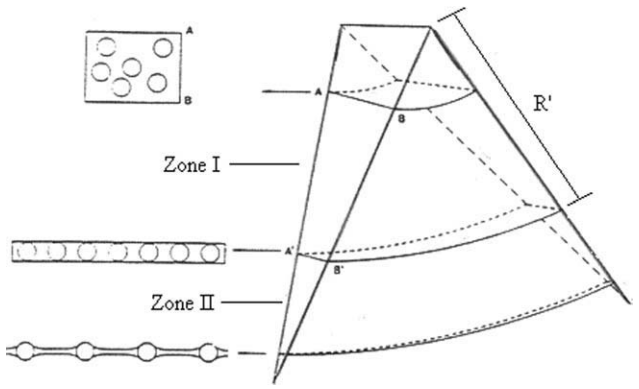

Figure 13. 3-D sketch of a portion of the thinning sheet containing particles.

A plan view of the cross section at increasing distance from the orifice of the nozzle is shown on the left-handed side (L.H.S).

(Dombrowski and Fraser[3]). However, where the particles are wetted, i.e., where the contacts angles are less than 90°, the interfacial energy, which is in excess of the thermal energy, would be required to strip water off the particles.[11]

The interfacial energy at the glass–water interface is in the region of 50–70 $\times$ 10^{-3} N/m. Those of the particle–water interface, where particles are clays, are likely to be higher because of the physical and chemical interaction of the particle surfaces with water. Using the above estimates of surface energies, it can be shown that the energy per mole required for breaking the hydrogen bonds at the water–particle interphase is about 1000 times greater than the kinetic energy per mole of the water, imparted at the nozzles in typical atomization work. Therefore, traction due to the mechanical energy imparted at the nozzle cannot account for the perforation process.

The sheets produced in this work are continuous in the axial direction and move at high velocities and, therefore, the residence time in the sheets are small (of the order of 0.1 μs); therefore, gravity drainage is negligible.

Thus, neither gravity nor mechanical energy imparted at the nozzle nor the thermal energy of the water would be sufficient to strip water from the particles. Furthermore, it was observed that sprayed particles (clay, glass, and *Lycopodium*) remained wetted.

Cell droplet model

In the light of the above, it is necessary to explore a hydrodynamic explanation for the observations, which is well established in the fluid dynamic literature.

In analyzing the likely effects of particles on sheet stability, it is instructive to consider the structure of the sheets as comprising two zones: zone I, where the sheet thickness is greater than that of the particles and zone II, where the sheet thickness is less than that of the particles.

Figure 13 shows a 3-D sketch of the expanding sheet with the zones identified. In the absence of wave thinning, the radial distance (R') at which zone I ends and zone II begins depends on the particle size, d, and can be estimated from Eq. 1 to give:

$$R' = \frac{K}{d} \tag{3}$$

Within zone II, the sheets can be conceptualized as comprising "cells" of liquid with bulbous ends, bordered by particles which move apart due to extensional flow (see the sketch Figure 13). The dynamics of the liquid in the "cells" would be similar to that of planar drops with bulbous ends as described by Taylor,[12] Buckmaster and Flaherty,[13] Acrivos and Lo,[14] Rallison and Acrivos,[15] Stone and Leal.[16] Motion arising from the excess pressure gradient due curvature variations would be resisted by viscous forces.

Taylor[12] identifies two dynamical consequences of the imposition of extensional flow on the drop.

If the convective term due to elongation is dominant then the dynamics will be similar to that of an inviscid liquid drop; hence, long extensions will be achieved producing long thin segments in the midsection. Under these circumstances, curvature induced thinning will not be intense enough to cause puncture. This result is confirmed by Acrivos and Lo[14] who showed by calculation that when the imposed elongational flow is high and convective terms dominate then the drops will not break-up, instead they will form long slender bodies with thin midsections.

When the Reynolds number for elongation is small then the dynamics of the evolution of the drop is dominated by viscous flows accompanied by intense localized thinning, which cause the drops to develop bulbous ends and burst. These results are confirmed by Buckmaster and Flaherty,[13] who studied the dynamics of the relaxation of pre-extended planar droplets, and found that curvature variations imposed by the bulbous ends give rise to large velocities gradients leading to bursting. Stone and Leal[16] show that once drops have attained certain shapes (a degree of curvature variation), eliminating the imposed flow cannot prevent bursting. Rallison and Acrivos[15] define as this type of drop break-up as type 1 bursting.

The presence of curvature variations on the sheets is illustrated in Figure 14, which shows a sketch of the profile of "cells" in zone II before and after extension. The constraints at the boundaries lead to the development of a convex region between A and B, followed by a concavity between B and C. According to the symmetrical boundary conditions, the curvature is zero at centre of the "cell" (D). The particles at the ends of the "cells" undergo rigid body motion and cannot deform to take up the stresses, unlike the normal drop with deformable ends. Therefore, the curvature driven flow is likely to be more intense and persist throughout the lifetime of the "cell" compared with what would obtain in bulbous drops of pure liquids, which can develop pointed ends to dampen curvature effects.

Parameters of "cell" elongation

Whereas the mathematical analysis of evolution of the liquid thickness profile in the "cell" lies beyond the scope of this experimental article, some useful remarks can be made about the dynamics of the process at the qualitative level by considering the role of the pertinent dimensionless numbers. The Reynolds number would determine the relative importance of convective terms to viscous terms in the Navier-Stokes equation for describing the dynamics of the extension of the "cells."

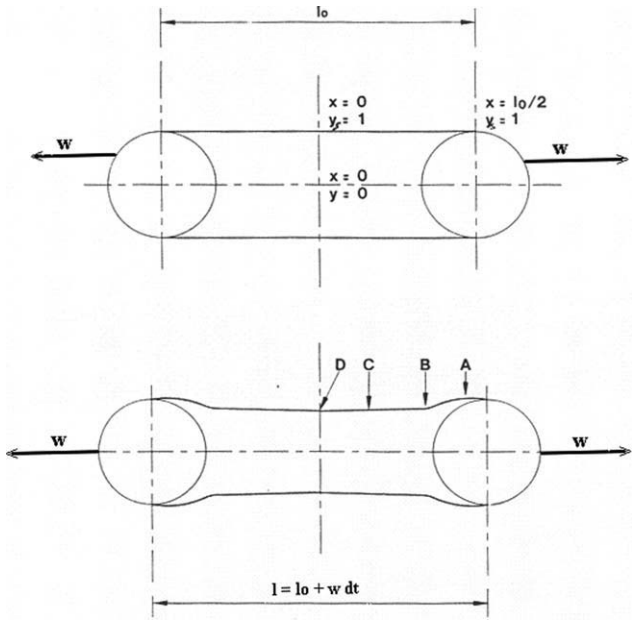

Figure 14. Schematic of the liquid profile within a "cell" before and after elongation by *w·dt*.

The nominal Reynolds number for cell elongation is given by:

$$Re = \frac{\rho w a}{\mu} \tag{4}$$

where w is the speed with which the particles recede from one another and a is the characteristic length. The speed with which particle centers recede is given by:

$$w = -U\Theta, \tag{5}$$

where Θ is the angle subtended at the source of sheet by two neighboring receding particles a distance ℓ apart. Θ is given by:

$$\Theta = \ell/\mathrm{R} \tag{6}$$

The lengths of the cells are subject to random perturbations and so are the speeds at which particles recede from one another. However, the average value of the interparticle distance $\overline{\ell}_0$ at the border between zones I and II can be estimated from phase balance. Thus, consider a slab of suspension at the point where the sheet thickness equals the particle size and which is one particle diameter wide! Suppose such a slab contains N noninteracting particles, separated by the distance ℓ_0 at the border between zones I and II. In principle ℓ_0 is a distributed parameter; however, if N is large, the expected value of ℓ_0 is the average value, $\overline{\ell}_0$.

The volume of the slab of fluid $= (N-1)\overline{\ell}_0 dxd$

The volume of particles $= N\pi\frac{d^3}{6}$

From phase balance, the volume fraction of particles is given by:

$$\psi = \frac{N\pi d^3}{6(N-1)\overline{\ell}_0 d^2}$$

From which the average interparticle spacing is given by: $\overline{\ell}_0 = \frac{N}{(N-1)}\frac{\pi d}{6\psi}$, which in the limit where N is large approaches,

$$\overline{\ell}_0 = d\left[\frac{\pi}{6\psi}\right] \tag{7}$$

Substituting Eqs. 3, 6, and 7 into Eq. 5 gives:

$$w = d^2\left[\frac{\pi}{6\psi}\right]\frac{U}{K} \tag{8}$$

Thus, the speed with which particles recede from one another decreases with increasing volume fraction of solids.

Reynolds number for "cell" elongation

Substituting the above into Eq. 4 gives the expression for the "cell" elongation Reynolds number below, which falls rapidly with diminishing particle size and increasing volume fraction of solids.

$$Re = \frac{\rho d^2 a}{\mu}\frac{\pi U}{6\psi K} \tag{9}$$

The particle diameter can be used as the characteristic length scale, a, for cell elongation; however, when the interparticle distance $\overline{\ell}_0$ which is the appropriate value (Stone and Leal[16]) is used, a greater dependence of volume fraction is predicted as below.

$$Re = \frac{\rho d^3}{\mu}\frac{\pi^2 U}{36\psi^2 K} \tag{10}$$

It can be inferred from the above that at low-phase ratios the Reynolds number would be higher; therefore, the dynamics of elongation would be dominated by the convective terms instead of the viscous term in the Navier-Stokes equation. From the analogies with the evolution of planar drops in extension flow, the dynamics would be similar to that of an inviscid liquid drop undergoing elongation. Long extensions would be achieved, producing thin segments in section C (beyond B) in Figure 14. Thus, the sheets would be thinner in these regions than would be expected from the bulk extensional flow. Under these circumstances, the liquid medium is supplied at high velocity to satisfy any pressure gradient produced by the local curvature gradients. Curvature induced thinning will not be intense enough to cause localized puncture in the life time of the sheet; therefore, no perforations occur in spite of the presence of particles at low-phase ratios.

The stability of the sheets of suspensions of low-volume fraction of coarse particles (as measured by break up length), will be controlled by the accelerated growth of waves, in the thin sections of the "cells," leading to shorter sheets as observed in this work.

The elongation of the "cells" at low Reynolds numbers present a necessary but not sufficient condition for bursting or perforation.

Validation of the cell droplet model

Shadow Photographs of Sheets in Zone II. The observed magnification of particles in the sheets confirms the presence

of curvature variations on the liquid surface between particles within Zone II. This is caused by particles holding water around them due to surface tension force. Therefore, the near flat sheet becomes distorted by particles some distance away. Light passing through the region of distortion cannot be focused on the film by the camera lens. Such areas develop as high-contrast regions on the photographic film as if particles extended that far leading to apparent magnification of suspended particles. It follows that liquid is unevenly distributed in the interparticle space. Some areas will be much thicker than the average thickness of the sheet at that radial distance, whereas others would be much thinner.

The increase in the magnification of the particles by the liquid-lens effect described above—with increasing distance within zone II (as summarized in Figure 9) is entirely consistent with this model as the local distortion of the sheet by particles can be expected over a wider area as the sheet thins with increasing radial distance from the nozzle.

Shadow photographs of sheets containing Glass II indicate that zone II begins closer to the nozzle for these particles compared with the distance at which it would begin for particle of size equal to the mean value (as would be estimated by Eq. 3). This is because a significant proportion of the particles have sizes greater than the mean or modal values. Examination of the picture in Figure 5B shows that the black patches appear closer to the nozzle in the region where sheet thickness is about 80 μm. This is caused by the presence of particles of this size in the distribution shown in Figure 1A.

Thinning Rates and Curvature Driven Flows. We consider in this section, the kinematics of "cell" droplet evolution in time. The average thinning rates of the sheet due to extension flow imparted at the nozzle can be predicted from the thinning parameter. However, particle induced thinning rates are difficult to measure directly, but are inferred from the kinetics of perforations.

Using the *Lycopodium* experiments as a model, the observation that perforation originate at about 2.7 mm inside zone II imply that the curvature variations do cause segments liquid within the interparticles space to thin locally from the average value (27 μm) to ultrathin values (0.1 μm) over a period of 12 ms. Thus, curvature driven localized thinning rate is about 0.22 m/s. The thinning rate imposed by the extensional flow falls with radial distance according to Eq. 15. At the border between zone I and II produced by Nozzle N521, it is about 6 times lower (0.038 m/s) than the above and about 9.5 times lower than the curvature driven thinning in sheets produced by the larger nozzle (N943). In the absence of waves, extensional flow produced by the nozzles (e.g., N521) would require a much longer residence times (>78 ms) to reduce the thickness of sheet to ultrathin values.

$$\frac{dH}{dt} = \left(\frac{K}{R^2}\right) U \tag{11}$$

In other words, within the perforation regime, localized thinning within the "cells" is an order of magnitude greater than that due to motion imposed on the sheet by the nozzle. The implications of this on the kinematics of droplet evolution are discussed further.

To further explore the relationship between the observed thinning rates and the curvature induced velocities, we consider a slab of liquid in Zone II some distance away from the nozzle orifice. The thinning and stretching (extension) can be represented in two-dimensional rectilinear axes: x-axis is in the direction of extension and the y-axis is perpendicular to the sheet. The slab extends from $-h$ (lower free surface) to h (upper free surface) on the y-axis and 0 to x along the x-axis, where h is the half thickness of the sheet. As the slab is stretched it thins. The continuity equation is thus:

$$\frac{\partial u}{\partial x} = -\frac{\partial v}{\partial y}, \tag{12}$$

where u and v are the velocities along x-axis and y-axis, respectively. We integrate both sides of the continuity across the local half thickness of the sheet, after the method of Levich[17] and Pozrikidis,[18] in analyzing the flow of slender or thin liquid bodies, to give:

$$\frac{\partial}{\partial x}\int_0^h u\partial y = -[v]_0^h = -(v_{y=h} - v_{y=0}) = -v_{y=h} = -\frac{dh}{dt};$$

From the symmetrical boundary condition, $v_{y=0} = 0$. The integral in the left hand side of the above is by definition the average material flux, $\overline{hu}$. Thus

$$\frac{\partial hu}{\partial x} = -\frac{dh}{dt}. \tag{13}$$

By taking the ratio of both sides of the equations in the presence of particles (subscripted 2) to the same quantities in the absence of particles (subscripted 1) and noting the ratios of thinning rates deduced from the experiments we obtain, beyond the radial distance at which zone II begins, gives the following:

$$\frac{\left[\frac{\partial \bar{h}\bar{u}}{\partial x}\right]_2}{\left[\frac{\partial \bar{h}\bar{u}}{4\partial x}\right]_1} = \frac{\left[\frac{dh}{dt}\right]_2}{\left[\frac{dh}{dt}\right]_1} \geq 6 \text{ to } 10.$$

The order of magnitude of the ratio of the velocity gradients can be inferred from the ratio of fluxes by noting that the local thicknesses, h, start from the same value but rapidly approaches zero in the perforation regime, but changes little in the absence of particles. Thus the ratio $\overline{h_2}$ to $\overline{h_1}$ over the perforation period is 2. The ratio of velocity gradients is given by:

$$O\left\{\frac{\left[\frac{\partial \bar{u}}{\partial x}\right]_2}{\left[\frac{\partial \bar{u}}{\partial x}\right]_1}\right\} \approx \left(\frac{\overline{h}_1}{\overline{h}_2}\right) O\left\{\frac{\left[\frac{\partial \bar{h}\bar{u}}{\partial x}\right]_2}{\left[\frac{\partial \bar{h}\bar{u}}{\partial x}\right]_1}\right\} \geq 12 \text{ to } 20$$

Thus, the ratio of velocity gradients in the presence of particles to those in the absence of particles also exceeds 6. These results are in agreement with the evolution of drops with bulbous end reported in the literature. Buckmaster and Flaherty[13] observed from calculations that two-dimensional drops will burst even when the external flow field is relaxed, provided the bulbous shape had developed beyond a certain degree. In this work, the particles at the ends of the cells are

wetted and not deformable; therefore, the curvature variations exerted on the sheets by them are expected to be severer than what one would expect in bulbous drops without particles. Thus, particle induced curvature driven flow is more intense than that due to extension flow and that could explain the observed insensitivity of perforation (distance and critical phase ratio) to the nozzle (value of K) used and to the ejection pressure (ejection velocity U) in this work and also in work reported in the literature.[3]

Critical perforation phase ratio of "cells"

It is important for the experimentalist or the design engineer, to be able to predict what the critical perforation phase ratio is, so that he can decide on how to formulate suspensions for atomization, which will form sheets which break up to give the desired droplet sizes. The results of the experiments presented in this work show that particle size is important in imposing curvature variations on the sheet and that this is the driving force for perforation. In response to the above, the liquid shears and breaks, therefore the pertinent suspension properties are: surface tension (σ), density (ρ), and viscosity (μ) of the liquid and the size of the particles (d). The atomization velocity is excluded because the as argued above its effect on thinning within the cells is negligible compared with curvature driven flow. The density of the particles is also not relevant to the perforation process, as demonstrated by the similarity the observed disintegration of sheets of suspensions of glass particles and *Lycopodium* particles despite the over two-fold difference in the particle densities (2.5 g/cc to 1.1 g/cc, respectively).

We use dimensional analysis to summarize the relationship between the critical phase ratio and the above properties of the suspensions, thus:

$$\psi_c = \mu^{n1} d^{n2} \rho^{n3} \sigma^{n4}$$

Equating powers of the dimensions on both sides of the equation gives:

Powers of mass:

$$0 = n1 + n3 + n4$$

Powers of length:

$$0 = -n1 + n2 - 3n3$$

Powers of time:

$$0 = -n1 - 2n4$$

From the above, the relationships between the powers of the variable are:

$n2 = -\frac{1}{2}n1$, $n3 = -\frac{1}{2}n1$, $n4 = -\frac{1}{2}n1$. Because of the observed positive correlation of the critical phase ratio, in Figure 12, with increasing particle size, only values of $n1$ less than zero need be considered. Substituting values permissible values of $n1$ in the above relationships yields equations which predict the dependence of the critical phase ratio on the suspensions properties. Thus for the case where $n1 = -1$,

$$\psi_c = \frac{A_c}{\mu}\sqrt{d\rho\sigma}. \tag{14a}$$

For the case where $n1 = -2$,

$$\psi_c = \frac{A_c}{\mu^2} d\rho\sigma \tag{14b}$$

A plot of Eqs. 14a and 14b in Figure 12 shows that the data is better described by Eq. 14a than Eq. 14b and that the best estimate of A_c determined from experiments is 5×10^{-3}. The appropriateness of Eq. 14a was confirmed from discriminating experiments which showed that the critical perforation phase ratio of suspensions of *Lycopodium* in water–glycerol mixture of viscosity twice that of water, 2 cP, fell from about 22% to 13%. Decreasing the surface tension by the addition of ethanol to the water medium also decreases the critical perforation phase ratio as predicted.

By analogy with the break-up of bulbous drops, it can be inferred from Eq. 14a that the dimensionless perforation number, A (in Eq. 15), whose critical value is A_c, is a measure of the curvature capillary number, or the tendency for "cells" to burst.

$$A = \psi\mu\sqrt{\frac{1}{d\rho\sigma}} \tag{15}$$

Stability of sheets containing medium and coarse particles

The trends in the stability of sheets containing coarse noninteracting particles shown by curves C, D, E, and F in Figure 8A and curve A, B, C, and D in Figure 8B can be directly inferred from the model described above. The size of such particles is such that Zone I of sheets containing them, would lie close to nozzle, in the region of the sheet where normal aerodynamic waves would be underdeveloped. In this work, medium and coarse particles comprise *Lycopodium*, Glass I, and Glass II. The ratio of the momentum force to viscous force (Reynolds numbers) for "cell" elongation along curves C′ and E′ in Figure 7A and curves A′ and C′ in Figure 7B decrease with increasing phase ratio as summarized in the Table 6 below. As explained in the sections above, the convective terms in the descriptive equations decrease in importance as viscous terms increase leading to increasing localized thinning of the midsections of the "cells" due to curvature driven flow. As a consequence, the axial waves would "see" a succession of "cells," which thin at rates far in excess of that imposed by the radial flow. According to Squire's[9] theory, the growth rate of wave is inversely proportional to the square root of the local sheet thickness, therefore the waves will grow faster in zone II, and will require smaller amplitude ratios than otherwise would be the case, to break-up the sheets. These two effects reinforce one another and thus the break-up lengths of the sheets decrease with increasing phase ratio on the above curves. Figure 10 confirms the reduction in the amplitude of the waves, which break-up the sheets containing coarse particles, with increasing phase ratio even though the sheet thickness at the break-up point increases as the sheets become shorter.

Table 6. Summary of Pertinent "Cell" Parameters Underlying Sheet Stability

Curve	Particles	Nozzle	Range of "Cell" Reynolds Numbers	Range of "Cell" Perforation Numbers	Growth Time of Waves as Percentage of Growth Time of Equivalent Sheet of Water
Figure 7A, Curve A	Fine glass (III)	N521			
Figure 7A, Curve B	Fine glass (III)	N521		>5 E −03	
Figure 7A, Curve C	Glass II	N521	5427–14		18%
Figure 7A, Curve D	Glass II	N521		>7 E −03	
Figure 7A, Curve E	*Lycopodium*	N521	1500–13		8%
Figure 7A, Curve F	*Lycopodium*	N521		>6.5 E −03	
Figure 7B, Curve A	Glass II	N943	5124–61		15%
Figure 7B, Curve B	Glass II	N943		>6 E −03	
Figure 7B, Curve C	Glass I	N943	11,236–46		13%
Figure 7B, Curve D	Glass I	N943		>6 E −03	

The perforation number increase with increasing phase ratio. However, perforation only occurs along curves B′, D′, and F′ in Figure 7A and curves B′ and D′ in Figure 7B on the sheets containing coarse particles, when the values are greater than the critical value of about 3.7×10^{-3} as shown in Table 6 above. This agrees with the simple model presented above. The observed mild reduction of perforation distance with increasing phase ratio in Figures 7A (curves D′ and F′) and B (curves B′ and D′) reflect the expected reduction in the average inter particle distance of the ''cells'' as phase ratio increases and therefore the intensification the impact of the curvature driven flow on the sheet with increasing phase ratio, which would reduce elongation time before rupture.

The relative insensitivity of the perforation distance of sheets containing coarse particles to ejection pressure for a given sheet thickness parameter (see Table 3), indicate that the speed with which neighboring particles separate (which is proportional to the sheet velocity) play a less important role in the perforation process than the curvature driven flow induced by particles in zone II. By analogy with the break-up of planar droplet with bulbous ends the curvature capillary number would be high and instability in the form of spontaneous perforations originate only a short distance into zone II. Pandit and Davidson[19] in their study of the hydrodynamics of bubble rupture find the spontaneous break occurs when the thickness is of the order of 0.09 μm. Madarelli[20] shows that ultrathin films rupture spontaneously due to disturbance on the molecular scale when the thickness is less than 0.1 μm. In this work, perforation can be attributed to the development of ultrathin films in the interparticle space, which cause rupture by similar mechanism.

The prediction of the critical phase ratio as a function of particle size, in Eq. 14a, is plotted in Figure 12, using the properties of water and the mean particle size for d, to show that the observed experimental results agree with the predicted trend for the coarse particles. The greatest deviation between the observed and the predicted critical phase ratios occur at the fine particle range. Whereas normal disturbances from the nozzle, which are believed to be the source of normal aerodynamic waves, would have a growth time in the region of 0.3 ms before reaching the border of zone II for sheets containing coarse particles produced by either nozzles; when the same nozzles are used to produce sheets containing fine particles (Glass III), growth time of waves before reaching Zone II are much larger and lie between 1.3 to 1.7 ms. Thus, waves of significant amplitudes can be attained, which would make the prediction in Eq. 3 only approximate.

Waves

Although this work has not been concerned with measuring the growth rate of waves, the impact of particles on the appearance of mature waves in zone II deserves comment. Conventional atomization theory predicts that wave growth rates on liquid sheets are retarded by increased bulk density and viscosity but increases with the reduction in sheet thickness. In zone I, the axial waves ''see'' a sheet whose thickness is determined by bulk expansion (Eq. 1).

The early appearance of waves (see Figure 4) and the reduced break-up lengths of nonperforated sheets (Figures 6A, B) confirm that in zone II the waves ''see'' a succession of elongating ''cells'' which thin at a rate greater than that predicted in Eq. 1 due to curvature driven flow and that the growth rate of waves is determined by the thinnest regions in the interparticle space. As stated in the previous section, the thinning rate due to curvature driven flow can be as much as 6 times higher than that due to bulk elongation thus leading to much larger growth rates of waves in zone II.

Stability of sheets containing fine particles

Where fine particles are use in preparing the suspensions, the limit of Zone I as predicted from sheet expansion, would lie at a longer radial distance from the nozzle such that conventional atomization theory would predict the growth of sinuous waves to significant amplitudes. Clark and Dombrowski[21] predict that the waves thin the sheet to a maximum degree in troughs at half wavelength intervals. In situations where the length of Zone I, as predicted by Eq. 3, is sufficiently distant from the nozzle for waves to grow to high amplitudes, then the sheet thickness in the troughs of the waves could fall below the size of the particles inside zone I. Sheet made from suspensions of Glass III fall into this category. Waves grow within Zone I to an extent that at the average sheet thickness of 7 μm, the troughs of the waves have a thickness of less than 5 μm. For demonstrative purposes, wave thinning due to varicose waves have been sketched Figure 15. The heavy solid lines represent the

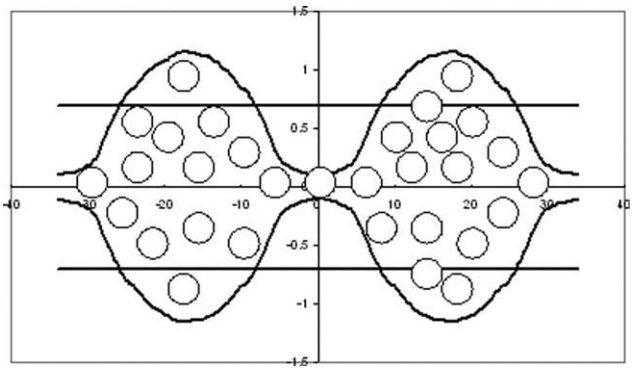

Figure 15. Sketch of profile of a sheet of suspension of fine particles showing disturbance by high-amplitude waves.

position of the undisturbed surfaces of the sheet in the absence of waves. The varicose waves have grown to the extent that the thicknesses of the troughs are less than the particle size. This demonstrative calculation sketched above agrees with the observations of the perforation of sheets containing fine particles (see Figures 5C and 6A). The sheet perforates closer to the nozzle than would be predicted by Eq. 3. Quite clearly, the estimate of the critical perforation number, as presented above, can at best be approximated because of the concurrent action of the waves and the curvature driven sheet thinning.

The perforation number increases with phase ratio, however, as in the case of the sheets containing coarse particles, perforation along curve B′ in Figure 7A, on sheets containing fine particles when the perforation number is greater than 5.3 E −03. The latter experimentally observed number is less than but close to the derived value because of the interference of aerodynamic waves, which are present on these sheets, well before Zone II, (as estimated by Eq. 3), is reached.

Effect of particle size on sheet stability

The radial distance at which perforations occur is strongly dependent on the particle size, because curvature driven thinning commences at the point at which sheet thickness falls below particle size. This is demonstrated by the pictures in Figure 6. A useful way of predicting the approximate position of the radial perforation length is to assume that it occurs close to the border between zone I and II and to use Eq. 3 in the estimation. The plot shown in Figure 11 supports this argument, although it is worth noting that whereas the points representing coarse particles lie above the predictive curve, that of the fine particle lies below it. This is because waves interfere with the perforation process of sheets containing fine particles. The plot of the break-up length against reciprocal particle size deviates significantly from linearity because break-up is via wave action whose growth is accelerated by the particles.

Mixtures of particles sampled from different distributions

The model discriminatory experiment carried out with a suspension which is dilute in large particles but high in volume fraction of fine particles presents an interesting fluid dynamical paradox, which is illustrated in the sketch in Figure 16. At the point where the sheet thickness reduces below the size of the large particles through expansion flow, the sheet behaves like a dilute suspension. The ''cells'' formed by the large particles expand at a high Reynolds number; therefore, convection terms dominate the flow. In the example presented, the ''cell'' Reynolds number is about 958, and therefore, the sheet does not perforate near the point where the thickness falls below that of the large particles (0.006 m). Instead the midsections of the ''cells'' thin with particle separation to the point where the thickness in the inter particle space reaches the size of the small particles. At that point, the ''new cells'' are formed by the fine particles, which expand at slower speeds, i.e., with a low Reynolds number. In the example presented in Table 5 and sketched in Figure 16, the Reynolds number of the new smaller ''cells'' is about 0.48. These new ''cells'' of liquid with bulbous ends, appearing closer to the nozzle than would be expected from the size of the fine particles, perforate the sheet because the dimensionless perforation number, A (5.4×10^{-3}), exceeds the critical value (5×10^{-3}). As shown in Table 5 above, the perforation distance is 0.0125 m, much shorter than the distance at which the average sheet thickness would fall below the size of the finer particles (about 0.05 m). The observed break-up length, 0.015 m, is also much shorter than that of the sheet containing fine particles but free of large particles is consistent with the explanation given above.

Break-up of sheets of structure forming suspensions

The observation of a wide range of sizes of agglomerates in the samples of the sheet collected in dispersant confirm that structure forming suspensions would break-up during passage through the high-shear zones in nozzle orifice to form agglomerate-particles suspended in a suspension of fines. The large agglomerates draw the water around them at the point where sheets thickness falls below the agglomerate size (15 μm of attapulgite). Beyond that point, the agglomerates separate creating thin sections which eventually fall below the size of the fines, which perforate the sheet. Thus, the sheets perforate at distances where the thicknesses, less than the size of the agglomerates 12.5 compared with 15–20 μm, but higher than those of the fines. Both the perforation distance and the break-up lengths are shorter that the

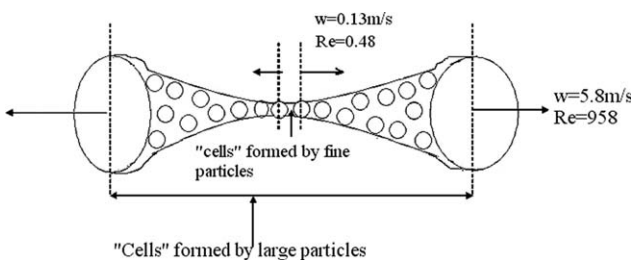

Figure 16. Sketch of section of sheet showing a "cell" formed by large particles at low-phase ratio and "cells" formed by fine particles at a higher phase ratio undergoing elongation.

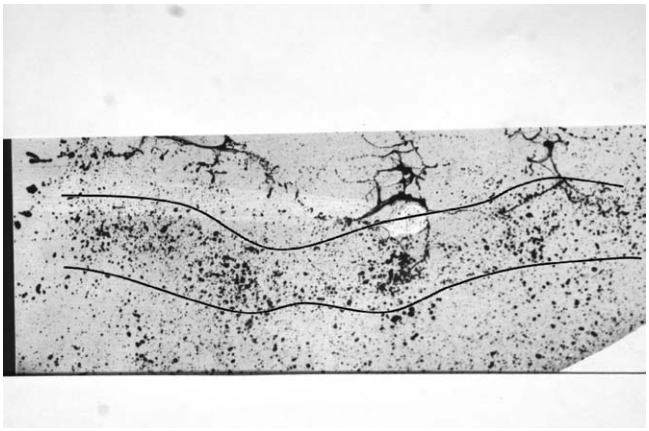

Figure 17. Photograph of a typical plume of droplets which results from the secondary disintegration of a sheet of water.

equivalent sheet of water. Thus, the break-up of sheets containing mixtures sampled from different particle size distribution may be used to model the break-up of suspensions of structure forming particles. The size and volume fraction of the agglomerate particles as well as the modified properties of the water medium are important for understanding the disintegration of such sheets. Yet often too little direct measurement is made of these parameters making prediction very difficult. Further work is required to shed more light on this interesting and important area of atomization of non-Newtonian (structure forming) suspensions.

Secondary disintegration of perforated sheets

Previous sections of this article describe the appearance of perforation on sheets during the primary process of sheet disintegration. As stated earlier, the perforations grow on the sheets resulting in a network of nodes which are joined by ligaments. Although no drop size measurements have been undertaken in this work, the observations of how the network of ligaments, formed above, breakdown to form drops in the secondary disintegration processes of drop formation are pertinent to the prediction of drop size distributions. This section describes the secondary disintegration of the network of ligaments into droplets.

Secondary processes in the formation of drops

Fraser et al.[4] postulate that portions of the sheets of the liquid, torn off by the axial waves during liquid atomization, contract into transverse cylindrical columns and are broken up by waves normal to the sheet according to Rayleigh's theory. Although there is no direct empirical evidence to support this hypothesis, we observed on the photographs of sheets of water undergoing disintegration a plume of droplets which extend across the entire span of the spray, which may be the result from this mechanism. An example of this observation is shown in the photograph in Figure 17 on which the plume is demarcated.

The secondary break-up of the network of ligaments containing the suspended particles differ from the above and deserve mention below. Figure 18 shows a picture of filaments of the suspension of the largest noninteracting particles (Glass I) undergoing secondary disintegration. A ligament linking two nodes which is undergoing break-up in three places is encircled in the above picture. Three types of drops would result from the above break-up. These are identified as: nodal drops, midsection drops and satellite drops in the above figure. It is expected that the particles would be found in the nodal and midsection drops, whereas the satellite drops would not contain any; as breaks in the filaments cannot occur across particles. The nodal drop gives rise to coarse droplets. Further discussion of the relative frequencies of the types of sprayed drop lies beyond the scope of this article.

Summary, Conclusions, and Recommendation

Sheet perforation

A deterministic and simple mechanism for the atomization of suspension of particles in liquids which accounts for the effect of particles on the disintegration of sheets produced by a hydraulic pressure nozzle has been put forward to explain the observations reported. Three driving forces tending to thin sheets (extensional flow, forces due to curvature variation and wave action) are identified. Sheet thinning, due to elongation, occurs at all radial positions and is similar to what pertains in sheets free of particles. Curvature forces become operational in the region where sheet thickness is less than particle size. The effect of this additional force is to destabilize the sheet locally at all phase ratios. Curvature-driven flow leads to sheet perforation at high-phase ratio for all particle sizes and the appearance of waves closer to the nozzles in sheets containing coarse particles compared with those free of particles.

Dimensional analysis is used to adduce the dependence of critical perforation phase ratio on particle size and the properties of the liquid medium.

Droplet formation process

Perforations grow as the portions of the sheet in between them contract to form nodes and ligaments. The elongational flow leads to breaks at the nodes and along the ligaments to form the nodal drops and the midsection drops. Satellite

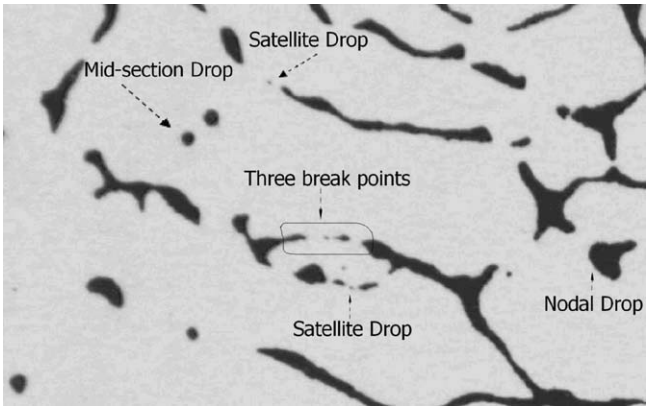

Figure 18. Secondary disintegration of network of ligaments formed by suspensions of particles of Glass I.

drops are formed at the breakage points. The break-up of the ligaments are similar to the break-up of pendant drops containing particles. As breaks do not occur across hard particles, satellite drops would normally not contain particles.

However, where you have submicron particles then they could be present in the satellite droplets although the agglomerate would not.

The major consequence of break-up closer to the nozzle when sheets are laden with particles compared with the case where they are free of particles is that droplets in the distribution which are labeled as nodal are larger because they originate at the point of perforation.

Whereas this work does not explore the quantitative effects of particle size distribution on drop size distribution, it can be inferred from the proposed mechanism and the evidence presented, that the inclusion of larger particles in suspensions can be used to control radial position where the sheets disintegrate and hence the drop sizes formed.

Acknowledgments

Dr. F. O. Addo-Yobo is grateful to Professor Norman Dombrowski, formerly of the University of Leeds, for painstakingly teaching him the Rear-Focused-Illumination photographic technique, which was used in this work and for introducing him to the world of atomization.

Literature Cited

1. Lefevbre AH. *Atomisation and Sprays*. New York: Hemisphere Publishing Corporation, 1989.
2. Chigier N, Meyer PL. *The atomization process in coal-water slurry sprays*. In *Proceedings of 8th International Conference on Coal/ Slurry Preparation*, Pittsburgh, USA, 1986:144–166.
3. Dombrowski N, Fraser RP. A photographic investigation into the disintegration of liquid sheets. *Philos Trans R Soc Lond Ser A*. 1953;247:101.
4. Fraser RP, Eisenklam P, Dombrowski N, Hasson D. Drop formation from rapidly moving liquid sheets. *AIChE J*. 1962;8:672–680.
5. Spielbauer TM, Aidun CK. The cause and origin of perforations in radially thinning liquid sheets. *J Liq Atomization Spray*. 1994;4:405–436.
6. Spielbauer TM, Aidun CK. The wave-thinning and breakup of liquid sheets. *J Fluids Eng*. 1994;116:724–734.
7. Mulhem B, Schulte G. Effect of solid particle characteristics on suspension atomization. *Atomization Sprays*. 2003;13:322–345.
8. Dombrowski N, Hasson D, Ward DE. Some aspects of liquid flow through fan spray nozzles. *Chem Eng Sci*. 1960;12:35–50.
9. Squire HB. Investigation of the instability of a moving liquid film. *Br J Appl Phys*. 1953;4:167–169.
10. Hagerty WW, Shea JF. A study of the stability of plane fluid sheets. *J Appl Mech*. 1955;22:509–514.
11. Binks BP, Horozov TS. *Colloidal particles at liquid interfaces: an introduction*. In: Binks BP, Horozov TS, editors. *Colloidal Particles at Liquid Interfaces*. Cambridge: Cambridge University Press, 2007:1–76.
12. Taylor GI. The formation of emulsions in definable fields of flow. *Proc R Soc Lond Ser A*. 1934;146:501.
13. Buckmaster JD, Flaherty JE. The bursting of two-dimensional drops in slow viscous flow. *J Fluid Mech*. 1973;86:625–639.
14. Acrivos A, Lo TS. Deformation and break-up of a single slender drop in extensional flow. *J Fluid Mech*. 1978;86:641–672.
15. Rallison JM, Acrivos A. A numerical study of the deformation and burst of a viscous drop in an extensional flow. *J Fluid Mech*. 1978; 89:191–200.
16. Stone HA, Leal LG. Relaxation and break-up of an initially extended drop in an otherwise quiescent fluid. *J Fluid Mech*. 1989;198:399–427.
17. Levich VG. *Physico-Chemical Hydrodynamics*, 1st ed. Prentice Hall, 1962:674–682.
18. Pozrikidis C. *Fluid Dynamics, Theory, Computation, and Numerical Simulation*, 1st ed. Kluwer Academic Press, 2001:424–428.
19. Pandit AB, Davidson JF. Hydrodynamics of the rupture of thin liquid films. *J Fluid Mech*. 1990;212:11–24.
20. Madarelli C. *The influence of the long range intermolecular interactions on the hydrodynamic stability of ultrathin film*. In: *Thin Liquid Film Phenomena, AIChE Symposium Series*, 1988;82:14–24.
21. Clark CJ, Dombrowski N. Aerodynamic instability and disintegration of inviscid liquid Sheets. *Proc R Soc Lond Ser A*. 1972;329: 467–478.

Manuscript received July 12, 2008, and revision received Aug. 29, 2010.